Available online at www.sciencedirect.com

SciVerse ScienceDirect

Acta Materialia xxx (2013) xxx–xxx

Acta MATERIALIA

www.elsevier.com/locate/actamat

Elucidating the variables affecting accelerated fatigue crack growth of steels in hydrogen gas with low oxygen concentrations

B.P. Somerday [a,b,*], P. Sofronis [b,c], K.A. Nibur [d], C. San Marchi [a], R. Kirchheim [b,e,f]

[a] Sandia National Laboratories, Livermore, CA 94550, USA
[b] International Institute for Carbon Neutral Energy Research (WPI-I2CNER), Kyushu University, 744 Moto-oka, Nishi-ku, Fukuoka 819-0395, Japan
[c] University of Illinois, Urbana, IL 61801, USA
[d] Hy-Performance Materials Testing, Bend, OR 97701, USA
[e] Institut für Materialphysik, Georg-August-Universität Göttingen, Göttingen, Germany
[f] Max-Planck-Institute for Iron Research GmbH, Düsseldorf, Germany

Received 9 March 2013; received in revised form 1 July 2013; accepted 2 July 2013

Abstract

The objective of this study was to quantify the effects of mechanical and environmental variables on oxygen-modified accelerated fatigue crack growth of steels in hydrogen gas. Experimental results show that in hydrogen gas containing up to 1000 v.p.p.m. oxygen fatigue crack growth rates for X52 line pipe steel are initially coincident with those measured in air or inert gas, but these rates abruptly accelerate above a critical ΔK level that depends on the oxygen concentration. In addition to the bulk gas oxygen concentration, the onset of hydrogen-accelerated crack growth is affected by the load cycle frequency and load ratio R. Hydrogen-accelerated fatigue crack growth is actuated when threshold levels of both the inert environment crack growth rate and K_{max} are exceeded. The inert environment crack growth rate dictates the creation of new crack tip surface area, which in turn determines the extent of crack tip oxygen coverage and associated hydrogen uptake, while K_{max} governs the activation of hydrogen-assisted fracture modes through its relationship to the crack tip stress field. The relationship between the inert environment crack growth rate and crack tip hydrogen uptake is established through the development of an analytical model, which is formulated based on the assumption that oxygen coverage can be quantified from the balance between the rates of new crack tip surface creation and diffusion-limited oxygen transport through the crack channel to this surface. Provided K_{max} exceeds the threshold value for stress-driven hydrogen embrittlement activation, this model shows that stimulation of hydrogen-accelerated crack growth depends on the interplay between the inert environment crack growth increment per cycle, load cycle frequency, R ratio and bulk gas oxygen concentration.

Keywords: Hydrogen embrittlement; Fatigue; Steel; Hydrogen gas impurities

1. Introduction

Concurrent cyclic loading and hydrogen gas exposure can lead to dramatically enhanced fatigue crack growth rates in ferritic steels, including lower-strength steels that are technologically favored for hydrogen production, storage, and distribution components. Suresh and Ritchie [1] established the foundation for understanding hydrogen-enhanced fatigue crack growth in lower-strength ferritic steels (yield strength <800 MPa). In their work crack growth rates were measured from the fatigue threshold (10^{-8} mm cycle^{-1}) to intermediate rates (10^{-3} mm cycle^{-1}) in both moist air and dry hydrogen gas. In two distinct crack growth rate regimes, i.e. at near threshold and intermediate growth rates, relatively higher rates were measured in hydrogen compared with air. In the near threshold regime elevated crack growth rates in hydrogen gas were attributed to diminished oxide-induced crack closure in

* Corresponding author at: Sandia National Laboratories, Livermore, CA 94550, USA. Tel.: +1 925 294 3141; fax: +1 925 294 3410.
E-mail address: bpsomer@sandia.gov (B.P. Somerday).

1359-6454/$36.00 © 2013 Acta Materialia Inc. Published by Elsevier Ltd. All rights reserved.
http://dx.doi.org/10.1016/j.actamat.2013.07.001

the dry, low-oxygen environment. In contrast, accelerated fatigue crack growth in the intermediate growth rate regime was induced by intrinsic hydrogen embrittlement mechanisms. Two salient characteristics of hydrogen-affected crack growth at intermediate rates are that the onset of acceleration is associated with a critical maximum stress intensity factor (K^T_{max}) and the crack path is intergranular.

As emphasized by Nelson [2] and Wei [3], activation of hydrogen embrittlement near an existing crack in a gaseous environment involves a series of sequential processes, for example (1) gas phase transport to the crack tip surface, (2) physical adsorption of the gas molecules, (3) dissociative chemical adsorption of the atomic species, (4) atomic hydrogen entry into the crack tip material, (5) diffusion of atomic hydrogen to the embrittlement site, and (6) hydrogen–material interaction leading to embrittlement and crack extension. This idealized scenario is germane to hydrogen-assisted crack growth in high-purity hydrogen gas environments. However, there is conclusive evidence that the embrittlement process can be inhibited by certain gas species, i.e. molecules composed of carbon, oxygen, and sulfur with unsaturated chemical bonds, when present in hydrogen gas [4]. The inhibiting function of these gas species is attributed to two characteristics: (1) the molecules adsorb on steel surfaces via dissociative chemisorption; (2) the carbon, oxygen, and sulfur atoms on steel surfaces impede hydrogen uptake [4]. Since inhibitor species disrupt the sequence of processes preceding the hydrogen–material interaction promoting hydrogen embrittlement, hydrogen-assisted crack growth is diminished in gaseous environments containing these inhibitors.

The objective of this study was to quantify the effects of mechanical and environmental variables on the inhibitor-modified accelerated fatigue crack growth of steels in hydrogen gas. Previous results demonstrate that oxygen can be a potent inhibitor of hydrogen gas-accelerated fatigue crack growth for steels [5–10], however, these studies did not define the limits of the mechanical and environmental variables that promote inhibition. In the work reported here fatigue crack growth rates were measured for a low-strength line pipe steel (X52) in high-pressure hydrogen gas as a function of the stress intensity factor range (ΔK), load cycle frequency, load ratio (e.g. mean stress), and oxygen concentration. The results show that inhibition is not absolute for the range of oxygen concentrations explored (<1–1000 v.p.p.m.). Rather, hydrogen-accelerated fatigue crack growth can be activated at each oxygen concentration under certain combinations of mechanical variables. The characteristics of hydrogen-accelerated fatigue crack growth appear similar to those described by Suresh and Ritchie for the intermediate growth rate regime [1]. To gain an insight into the mechanistic role of the variables affecting accelerated crack growth a model was developed based on the following premises: (1) prior to accelerated crack growth, i.e. during inert environment fatigue, oxygen is preferentially adsorbed on the new crack tip surface; (2) hydrogen uptake at the crack tip is limited by the extent of adsorbed oxygen; (3) the extent of oxygen coverage depends on the balance between the rate of fresh crack tip surface area exposure (i.e. crack growth increment per unit time) and the rate of diffusion-limited oxygen transport through the crack channel to this new surface. This model accurately captures the effects of the inert environment crack growth increment per cycle, load cycle frequency, load ratio, and bulk gas oxygen concentration on the onset of hydrogen-accelerated fatigue crack growth.

2. Experimental procedures

2.1. Material

The steel featured in this study was supplied as electric resistance welded (ERW) pipe (324 mm outside diameter, 12.7 mm wall thickness) which satisfied the API 5L Product Specification Level 2 (PSL2) for X52. According to a test report provided by the supplier (OSM Tubular-Camrose, Camrose, Canada) the yield strength and tensile strength of the base metal were 429 and 493 MPa, respectively. The reported steel composition is summarized in Table 1.

Optical metallography performed on the X52 steel base metal revealed that the predominant microstructure constituents were ferrite and pearlite. In addition, bands of inclusions were concentrated at mid-thickness in the pipe wall (Fig. 1). Based on a point counting method applied to micrographs representing the same plane as Fig. 1 the volume fraction of pearlite was estimated to be 7–10%.

2.2. Fatigue crack growth measurements

Fatigue crack growth rate testing on the X52 steel was carried out following procedures in ASTM Standard E647-05 [11]. Compact tension (CT) test specimens were extracted from the pipe at circumferential positions approximately 90° from the ERW seam. The specimens had the following nominal dimensions: thickness (B) 9.5 mm, width (W) 26 mm, and pre-crack starter notch length 5.3 mm. The specimens were designed with side grooves along the broad faces, which reduced the thickness in the crack plane (B_n) to 8.4 mm. The pre-crack starter

Table 1
Composition (wt.%) of the X52 line pipe steel as reported by the supplier.

C	Mn	P	S	Si	Cu	Ni	Cr	V	Nb	Al	Fe	CE[a]
0.06	0.87	0.011	0.006	0.12	0.03	0.02	0.03	0.002	0.03	0.034	Balance	0.11

[a] Carbon equivalent.

Please cite this article in press as: Somerday BP et al. Elucidating the variables affecting accelerated fatigue crack growth of steels in hydrogen gas with low oxygen concentrations. Acta Mater (2013), http://dx.doi.org/10.1016/j.actamat.2013.07.001

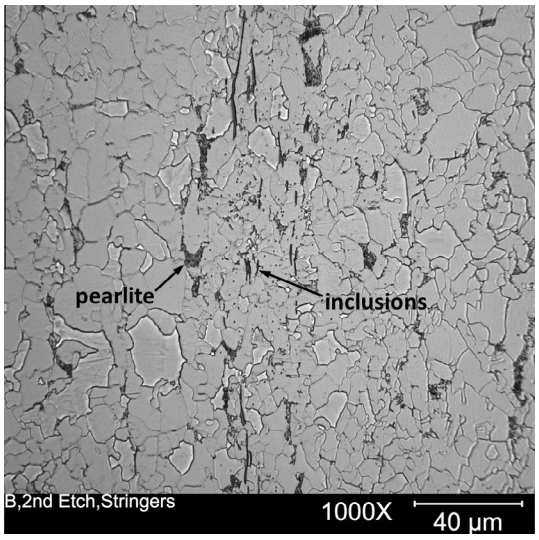

Fig. 1. Optical image of the microstructure of the base metal of X52 pipe (5% nital etch). The micrograph plane is parallel to the radial-circumferential plane of the steel pipe.

notch of the CT specimens was oriented parallel to the longitudinal axis of the pipe, i.e. the specimens were in the C–L orientation.

The CT specimens were prepared for testing by first ultrasonically cleaning the as-machined specimens in isopropyl alcohol. Following the procedures in ASTM Standard E647-05 a pre-crack was propagated from the starter notch in each specimen by applying cyclic loading. This fatigue pre-cracking process was conducted in air under the following mechanical conditions: load cycle frequency 15 Hz, R ratio (ratio of minimum load to maximum load) 0.1, and final maximum stress intensity factor (K_{max}) 7.5 MPa $m^{1/2}$. The pre-crack was propagated a distance of 1.8 mm from the notch tip to create a total pre-crack length to specimen width ratio (a_o/W) of approximately 0.27–0.28.

Fatigue crack growth tests were conducted on the X52 CT specimens in four different source gases: high-purity (99.9999%) hydrogen as well as hydrogen with 10, 100, and 1000 v.p.p.m. oxygen. This testing employed a custom designed apparatus consisting of a pressure vessel integrated into the load train of a servo-hydraulic mechanical test frame. Each pre-cracked CT specimen was placed in the pressure vessel and coupled to a pull rod penetrating through the bottom cover of the vessel. The pressure vessel was equipped with spring energized Teflon® U-cup seals to prevent gas leakage between the pull rod and bottom cover bore. After the pressure vessel had been assembled with the CT specimen inside the residual gas (e.g. air) was removed from the gas distribution manifold and pressure vessel using two different procedures. In preparation for the high-purity hydrogen source gas the pressure components were successively purged three times with high-purity helium gas (21 MPa pressure), evacuated once, then purged three more times successively with high-purity hydrogen gas (21 MPa pressure). In preparation for the mixed $H_2 + O_2$ source gases the protocol was modified to six consecutive purges with high-purity helium gas (21 MPa pressure) followed by one evacuation. Once these procedures were completed the pressure vessel was filled with the source gas to 21 MPa. No net load was applied to the CT specimen resulting from gas pressure acting on the end of the pull rod, since a secondary pressure chamber was designed into the vessel to ensure an equal and opposing force was applied to the pull rod. Each CT specimen was exposed to the source gas for less than 90 min prior to starting the fatigue crack growth test. All testing was conducted at ambient temperature (approximately 295 K).

Two fatigue crack growth test methods were applied to the X52 CT specimens in the hydrogen gas environments. In the first type of test the CT specimens were subjected to cyclic loading between fixed minimum and maximum loads (constant load amplitude) with a load ratio R of 0.1 or 0.5 and a load cycle frequency (f) of 10 Hz. This loading format led to increasing values of stress intensity factor range ΔK as the crack extended. The purpose of these tests was to measure the crack growth rate (crack growth increment per cycle da/dN) as a function of ΔK. In the second type of test the crack growth rate was measured at fixed values of ΔK. For these tests the load ratio was also constant ($R = 0.1$ or 0.5), but the load cycle frequency was varied in the range 0.001–10 Hz. These tests were designed to measure the da/dN vs. f behavior in each of the four hydrogen gas environments. At each frequency da/dN was measured over approximately 1 mm of crack extension, and multiple measurements were made on a single specimen. Only two specimens were employed for all constant ΔK test segments: one specimen was used for measurements in high-purity hydrogen and a second specimen was used for all measurements in the mixed $H_2 + O_2$ gases. For these latter tests, once the da/dN vs. f measurements for one environment were completed, the pressure vessel was purged and evacuated in preparation for the next $H_2 + O_2$ gas. These test segments started with the H_2 + 10 v.p.p.m. O_2 source gas and were completed with the H_2 + 1000 v.p.p.m. O_2 source gas.

For both fatigue crack growth test methods the loading and unloading rates were programmed to be constant in each cycle (i.e. triangular loading wave form) using an internal load cell as the feedback transducer in the control loop. Since the Teflon® seals impose friction forces on the pull rod the internal load cell ensured that loads applied to the specimen were measured directly. The crack opening displacement was measured using a linear variable differential transformer (LVDT) attached to the front face of the CT specimen. The hydrogen gas environments affected the output signal from the load cell strain gauges, leading to time-dependent, monotonic changes in the load reading. Since this spurious load increment was added to both the maximum and minimum applied loads the stress intensity factor range ΔK was unaffected. In contrast, the actual R ratio deviated from the programmed value, e.g. for nominal $R = 0.1$ actual values could vary from 0 to 0.2. The

Please cite this article in press as: Somerday BP et al. Elucidating the variables affecting accelerated fatigue crack growth of steels in hydrogen gas with low oxygen concentrations. Acta Mater (2013), http://dx.doi.org/10.1016/j.actamat.2013.07.001

Table 2
Hydrogen gas composition from selected fatigue crack growth tests.

Specimen no.	Source gas	Measured O_2 (v.p.p.m.)	Measured H_2O (v.p.p.m.)
FCG9	99.9999% H_2	<0.5	<0.5
FCG10	99.9999% H_2	<0.5	3
FCG5	99.9999% H_2	<0.5	6
FCG20	H_2 + 10 v.p.p.m. O_2	8	7
FCG19	H_2 + 1000 v.p.p.m. O_2	931	19
FCG21	H_2 + 1000 v.p.p.m. O_2	1030	21

LVDT output signal did not exhibit any significant time-dependent drift. Crack extension was quantified using the unloading compliance method. Load, crack opening displacement, and crack length data were digitally recorded at crack extension intervals of 0.13 mm. A commercial fatigue crack growth software product was used to control both the programmed loading and data acquisition.

The data analysis depended on the fatigue crack growth test method. For the constant load amplitude tests the crack growth rate da/dN was calculated by applying the incremental polynomial method in ASTM E647-05 to the crack length a vs. load cycle N data. The crack length data furnished by the unloading compliance method were corrected based on post-test optical measurements of the pre-crack and final crack lengths from the fracture surfaces. The difference between the crack lengths determined from unloading compliance and optical measurements were approximately 10–20% for the pre-crack and <1% for the final crack length. A routine in the analysis software linearly corrected the unloading compliance data so that the initial and final crack lengths equaled the optically measured values. For each da/dN value the associated ΔK value was calculated from the crack length and load range at the mid-point of the evaluated crack extension interval. For the constant ΔK tests the da/dN value in each 1 mm crack extension interval was calculated from the slope of a line fit to the measured a vs. N data. In each constant ΔK segment initial crack extension often exhibited transient behavior before reaching steady-state. The transient points were not included in the linear curve fit.

One variable that received particular attention was the actual composition of the hydrogen test gases. Although the high-purity source gas was certified as 99.9999%, some oxygen and water vapor contamination of the test gas was expected, since residual air cannot be completely removed from the pressure vessel. In addition, the mixed $H_2 + O_2$ source gases were supplied with individual certifications, but it was uncertain whether oxygen would be consumed over time to form water vapor. To address these issues, at the termination of selected tests in the high-purity and mixed $H_2 + O_2$ gases samples from the pressure vessel were collected in evacuated stainless steel bottles. These gas samples were then analyzed at a commercial laboratory, and the results are summarized in Table 2. For the high-purity hydrogen test gas oxygen was below the detection limit of 0.5 v.p.p.m., but water vapor levels up to 6 v.p.p.m. were measured. The oxygen concentrations in the mixed test gases did not significantly deviate from their specified levels in the source gas.

In addition to the fatigue crack growth tests in four different hydrogen environments, companion tests were conducted in ambient air. These CT specimens were prepared identically to those tested in the hydrogen environments. The test parameters in air included constant load amplitude or decreasing ΔK, $R = 0.1$ or 0.5, load cycle frequency = 10 Hz, and a sinusoidal load cycle wave form. The temperature and relative humidity in the ambient environment were approximately 295 K and 30–60%, respectively. A summary of all tests conducted in the hydrogen environments and ambient air is presented in Table 3.

2.3. Fracture surface characterization

Fracture surfaces from CT specimens tested in the hydrogen environments and in air were examined in a commercial scanning electron microscope. For specimens tested under constant load amplitude multiple areas were viewed along the crack growth direction so that evolution of the fracture surface features could be monitored as a function of ΔK.

Table 3
Summary of fatigue crack growth tests.

Specimen no.	Environment	Test method	R	Frequency (Hz)	No. of tests
FCG9, FCG13	99.9999% H_2	Constant load	0.1	10	2
FCG10	99.9999% H_2	Constant load	0.5	10	1
FCG5	99.9999% H_2	Constant ΔK	0.5	0.001–10	1
FCG17	H_2 + 10 v.p.p.m. O_2	Constant load	0.1	10	1
FCG20	H_2 + 10 v.p.p.m. O_2	Constant ΔK	0.1	0.1–10	1
FCG18	H_2 + 100 v.p.p.m. O_2	Constant load	0.1	10	1
FCG20	H_2 + 100 v.p.p.m. O_2	Constant ΔK	0.1	0.1–10	1
FCG19	H_2 + 1000 v.p.p.m. O_2	Constant load	0.1	10	1
FCG21	H_2 + 1000 v.p.p.m. O_2	Constant load	0.5	10	1
FCG20	H_2 + 1000 v.p.p.m. O_2	Constant ΔK	0.1	0.01–10	1
FCG7	Air	Constant load	0.1	10	1
FCG8	Air	Decreasing ΔK	0.1	10	1
FCG2	Air	Constant load	0.5	10	1

Please cite this article in press as: Somerday BP et al. Elucidating the variables affecting accelerated fatigue crack growth of steels in hydrogen gas with low oxygen concentrations. Acta Mater (2013), http://dx.doi.org/10.1016/j.actamat.2013.07.001

3. Results

3.1. Fatigue crack growth in high-purity hydrogen gas

The fatigue crack growth relationships da/dN vs. ΔK measured in high-purity hydrogen gas and ambient air at $R = 0.1$ and 0.5 are plotted in Fig. 2. Included in Fig. 2 are fatigue crack growth data measured in high-pressure nitrogen for X42 line pipe steel [12], which is a low-strength, ferrite–pearlite steel similar to X52. These data are nearly coincident with the da/dN vs. ΔK relationships measured for X52 in air. In the lower range of ΔK the da/dN vs. ΔK relationship measured in hydrogen at $R = 0.1$ coincided with the relationships measured in air or inert gas. As crack growth progressed under rising ΔK the slope of the da/dN vs. ΔK curve in hydrogen abruptly increased. These accelerating crack growth rates reach a level approximately one order of magnitude higher than the rates in air, then the slope of the da/dN vs. ΔK curve distinctly declined. Beyond this second slope change in the da/dN vs. ΔK curve the difference in crack growth rates between hydrogen and air was maintained at approximately one order of magnitude. The da/dN vs. ΔK relationship measured in hydrogen gas at $R = 0.5$ exhibited the same characteristics as the relationship measured at $R = 0.1$, i.e. multi-slope behavior and elevated crack growth rates compared with those in air. Although the da/dN vs. ΔK curves measured in hydrogen had similar features, the crack growth rates at $R = 0.5$ were notably higher than those at $R = 0.1$ over the entire range of ΔK.

The distinguishing features of the da/dN vs. ΔK relationships measured in high-purity hydrogen gas, e.g. an abrupt acceleration of crack growth rates above those in air or inert gas, multiple slopes, and an effect of the R ratio, are consistent with the work of Suresh and Ritchie [1]. Since the Suresh and Ritchie trends appear to prevail for X52 steel in high-pressure hydrogen gas one unexpected detail in Fig. 2 is the deviation of the da/dN vs. ΔK relationships in hydrogen at $R = 0.5$ and in air over the lower ΔK range. However, if the fatigue crack growth tests were started at lower ΔK the trends would likely follow the results of Suresh and Ritchie, i.e. at all R ratio values crack growth rates in hydrogen initially equal those in air, then abruptly accelerate.

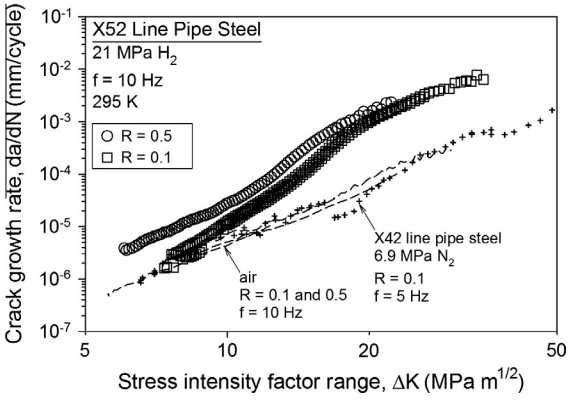

Fig. 2. Fatigue crack growth rate (da/dN) vs. stress intensity factor range (ΔK) relationships for X52 line pipe steel in high-purity hydrogen gas and ambient air. The da/dN vs. ΔK relationships in hydrogen and air were measured at both $R = 0.1$ and $R = 0.5$. Two datasets are plotted for high-purity hydrogen at $R = 0.1$. Fatigue crack growth data for X42 line pipe steel measured in high-pressure nitrogen gas [12] are included for comparison with the X52 data in air.

The distinct crack growth rate transitions for X52 steel in high-purity hydrogen gas are associated with changes in fracture surface features. At the onset of accelerated crack growth the fracture surfaces exhibited facets characteristic of intergranular crack growth (Fig. 3a). The proportion of intergranular facets increased as the crack growth rates accelerated under rising ΔK. The predominant intergranular crack growth then evolved into a transgranular crack growth mode (Fig. 3b). In the range of ΔK beyond the second slope change (Fig. 2) crack growth became exclusively transgranular (Fig. 3c). These intergranular and transgranular fracture surface features representative of hydrogen-assisted crack growth contrast with the transgranular features characteristic of crack growth in air (Fig. 4).

The da/dN vs. ΔK relationships in high-purity hydrogen gas (Fig. 2) were measured at a load cycle frequency of 10 Hz. The effect of load cycle frequency f on crack growth rates is illustrated in Fig. 5 for $R = 0.5$. For this data set the crack growth rate was measured at $\Delta K = 17.5$ MPa m$^{1/2}$ over the frequency range 0.001–1 Hz. At lower f from 0.001 to 0.1 Hz the crack growth rate was approximately constant. As f increased to 1 Hz the crack growth rate notably decreased by about a factor of two.

3.2. Fatigue crack growth in mixed H_2 + O_2 gases

The fatigue crack growth relationships measured in the mixed $H_2 + O_2$ gases at $R = 0.1$ exhibited similar characteristics to the relationships for high-purity hydrogen (Fig. 6). In particular, as crack extension progressed under rising ΔK crack growth rates in all hydrogen environments abruptly accelerated above the rates in air or inert gas. The most distinguishing feature of the da/dN vs. ΔK relationships in the mixed $H_2 + O_2$ gases was the effect of oxygen concentration on the transition point to accelerated crack growth. The da/dN vs. ΔK relationships for H_2 + 10 v.p.p.m. O_2 and high-purity hydrogen were essentially coincident. However, for the H_2 + 100 v.p.p.m. O_2 and H_2 + 1000 v.p.p.m. O_2 cases the onset of accelerated crack growth was displaced to higher ΔK values that depend on oxygen concentration. At these higher oxygen concentrations the initial hydrogen-assisted crack growth rates rose much more steeply compared with the analogous initial rates in H_2 + 10 v.p.p.m. O_2 and high-purity hydrogen. In addition, the terminal point of the initial steep rise in crack growth rates for the H_2 + 100 v.p.p.m. O_2 and H_2 + 1000 v.p.p.m. O_2 cases was defined by the curves for the higher-purity gases, i.e. the da/dN vs. ΔK relationships in all hydrogen environments ultimately converged.

Please cite this article in press as: Somerday BP et al. Elucidating the variables affecting accelerated fatigue crack growth of steels in hydrogen gas with low oxygen concentrations. Acta Mater (2013), http://dx.doi.org/10.1016/j.actamat.2013.07.001

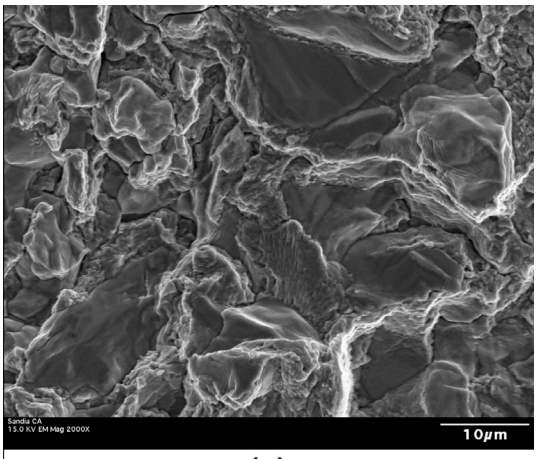

(a)

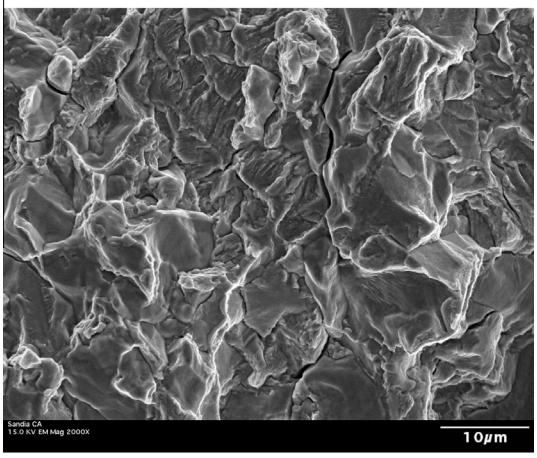

(b)

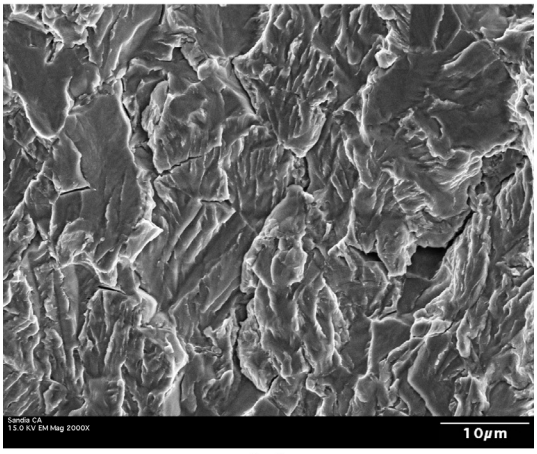

(c)

Fig. 3. Scanning electron microscope images of fracture surfaces from X52 line pipe steel tested at $R = 0.1$ and a frequency of 10 Hz in high-purity hydrogen gas. (a) Intergranular facets at the onset of accelerated crack growth ($\Delta K = 7.5$ MPa m$^{1/2}$). (b) Mixed intergranular and transgranular facets at a later stage of hydrogen-assisted crack growth ($\Delta K = 15.0$ MPa m$^{1/2}$). (c) Predominantly transgranular facets during hydrogen-assisted crack growth near test termination ($\Delta K = 28.0$ MPa m$^{1/2}$). The crack growth direction in the image is from bottom to top.

The da/dN vs. ΔK relationship measured in H_2 + 1000 v.p.p.m. O_2 at $R = 0.5$ was notably distinct from the

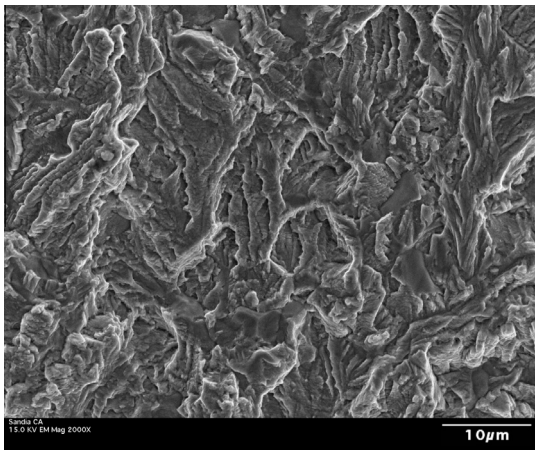

Fig. 4. Scanning electron microscope image of the transgranular fracture surface from X52 line pipe steel tested at $R = 0.1$ and a frequency of 10 Hz in air ($\Delta K = 7.5$ MPa m$^{1/2}$). The crack growth direction in the images is from bottom to top.

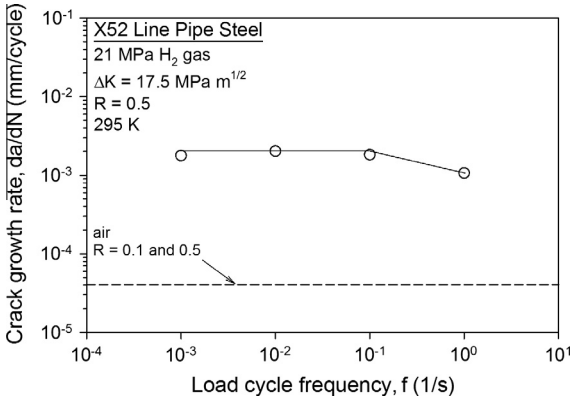

Fig. 5. Fatigue crack growth rate (da/dN) vs. load cycle frequency (f) for X52 line pipe steel in high-purity hydrogen gas at $R = 0.5$ and $\Delta K = 17.5$ MPa m$^{1/2}$. The crack growth rate in air at $\Delta K = 17.5$ MPa m$^{1/2}$ is shown for comparison. The solid line is not a curve fit but rather is intended to reinforce the data trend described in the text.

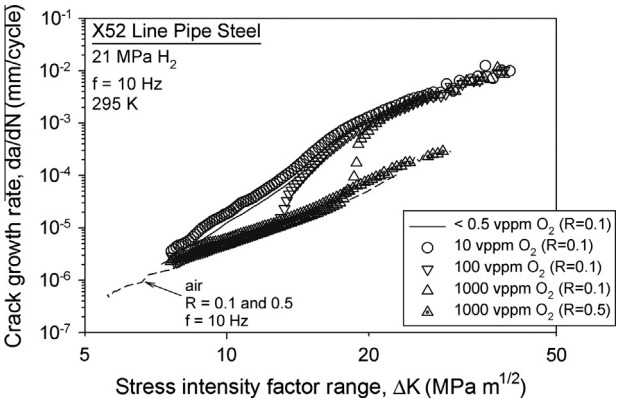

Fig. 6. Fatigue crack growth rate (da/dN) vs. stress intensity factor range (ΔK) relationships for X52 line pipe steel in mixed $H_2 + O_2$ gases ($R = 0.1$ or 0.5), high-purity hydrogen gas ($R = 0.1$), and ambient air ($R = 0.1$ and 0.5). The da/dN vs. ΔK relationships in high-purity hydrogen (<0.5 v.p.p.m. O_2) and air are from Fig. 2.

Please cite this article in press as: Somerday BP et al. Elucidating the variables affecting accelerated fatigue crack growth of steels in hydrogen gas with low oxygen concentrations. Acta Mater (2013), http://dx.doi.org/10.1016/j.actamat.2013.07.001

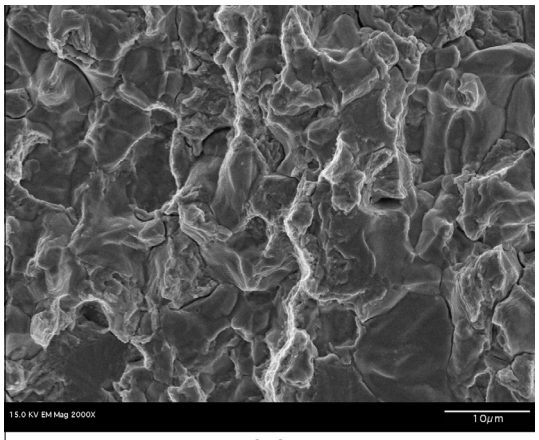

(a)

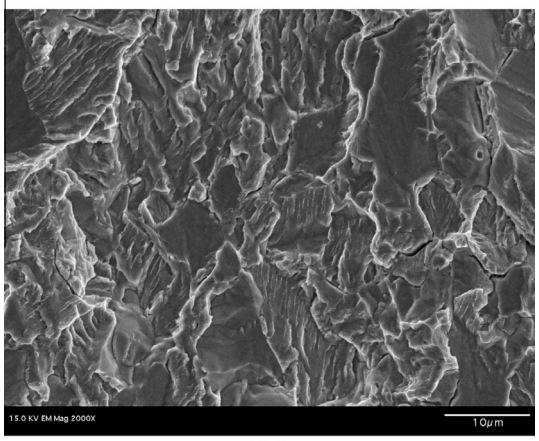

(b)

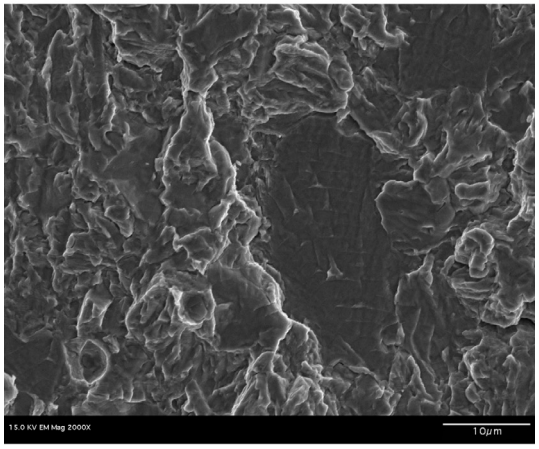

(c)

Fig. 7. Scanning electron microscope images of fracture surfaces from X52 line pipe steel tested at $R = 0.1$ and a frequency of 10 Hz in mixed $H_2 + O_2$ gas. (a) Intergranular facets at the onset of accelerated crack growth ($\Delta K = 13.0$ MPa $m^{1/2}$) in $H_2 + 100$ v.p.p.m. O_2. (b) Transgranular facets in a later stage of hydrogen-assisted crack growth ($\Delta K = 21.0$ MPa $m^{1/2}$) in $H_2 + 100$ v.p.p.m. O_2. (c) Transgranular facets at the onset of accelerated crack growth ($\Delta K = 17.5$ MPa $m^{1/2}$) in $H_2 + 1000$ v.p.p.m. O_2. The crack growth direction in the images is from bottom to top.

relationships measured in the various mixed $H_2 + O_2$ gases at $R = 0.1$ (Fig. 6). In particular, over the range of ΔK applied during the test crack growth rates at $R = 0.5$ coincided with those measured in air or inert gas, i.e. no crack growth acceleration was observed.

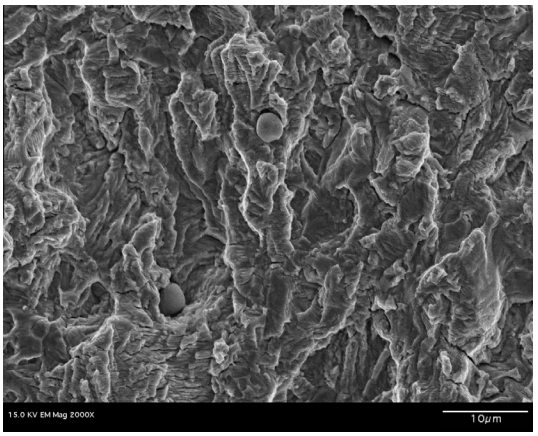

Fig. 8. Scanning electron microscope image of transgranular fracture surface from X52 line pipe steel tested at $R = 0.1$ and a frequency of 10 Hz in $H_2 + 100$ v.p.p.m. O_2 ($\Delta K = 12.0$ MPa $m^{1/2}$). The crack growth direction in the image is from bottom to top.

For tests at $R = 0.1$ the crack path at the onset of accelerated crack growth in the mixed $H_2 + O_2$ gases depended on the oxygen concentration. For the $H_2 + 10$ v.p.p.m. O_2 and $H_2 + 100$ v.p.p.m. O_2 cases the onset of accelerated crack growth was associated with intergranular cracking (Fig. 7a). Similarly to the behavior in high-purity hydrogen, the predominant intergranular mode transitioned to a transgranular mode (Fig. 7b) as hydrogen-assisted cracking progressed. In contrast, this transgranular cracking was observed from the outset for hydrogen-assisted crack growth in the $H_2 + 1000$ v.p.p.m. O_2 gas (Fig. 7c). For all mixed $H_2 + O_2$ gases and R ratios the crack path prior to accelerated crack growth was the transgranular mode (Fig. 8) characteristic of crack growth in air (Fig. 4).

The crack growth rate vs. load cycle frequency behavior in the mixed $H_2 + O_2$ gases ($R = 0.1$) was dramatically different compared with the behavior in high-purity hydrogen gas. In all of the mixed $H_2 + O_2$ gases the highest crack growth rates were at the highest load cycle frequencies (Fig. 9). In the $H_2 + 100$ v.p.p.m. O_2 and $H_2 + 1000$ v.p.p.m. O_2 gases crack growth rates immediately decreased to levels measured in air or inert gas as the frequency decreased from 10 to 1 Hz. These inert environment crack growth rates were maintained as the frequency was further decreased to 0.1 Hz. Similar trends were noted in the $H_2 + 10$ v.p.p.m. O_2 gas, but the abrupt transition to inert environment crack growth rates occurred at a lower frequency, i.e. between 1 and 0.1 Hz. The crack growth rates remained similar to those in air as the frequency further decreased to 0.01 Hz. It should be noted that the da/dN vs. f measurements in Figs. 5 and 9 represent a single ΔK level near 20 MPa $m^{1/2}$. This ΔK level was selected so that crack growth rates would be nearly identical in each hydrogen environment at 10 Hz (Fig. 6).

Please cite this article in press as: Somerday BP et al. Elucidating the variables affecting accelerated fatigue crack growth of steels in hydrogen gas with low oxygen concentrations. Acta Mater (2013), http://dx.doi.org/10.1016/j.actamat.2013.07.001

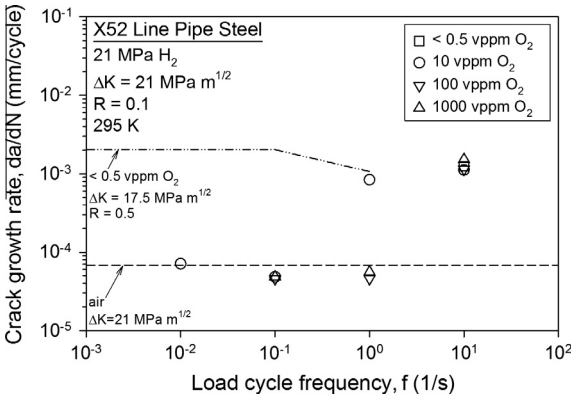

Fig. 9. Fatigue crack growth rate (da/dN) vs. load cycle frequency (f) for X52 line pipe steel in mixed $H_2 + O_2$ gases at $R = 0.1$ and $\Delta K = 21$ MPa m$^{1/2}$. The crack growth rate in high-purity hydrogen (<0.5 v.p.p.m. O_2) at 10 Hz and in air are shown for comparison at $\Delta K = 21$ MPa m$^{1/2}$. The trend line from Fig. 5 was included to contrast the da/dN vs. f behaviors in high-purity hydrogen and mixed $H_2 + O_2$ gases in the lower range of f.

4. Discussion

The trend in fatigue crack growth rate da/dN vs. stress intensity factor range ΔK (Fig. 2), as well as hydrogen-assisted intergranular fracture (Fig. 3a), observed for X52 line pipe steel in high-purity hydrogen gas was consistent with the results of Suresh and Ritchie [1]. In their study of fatigue crack growth in lower-strength ferritic steels exposed to low-pressure (0.1 MPa) hydrogen gas Suresh and Ritchie concluded that the onset of accelerated crack growth is associated with a threshold K_{max} value, i.e. K^T_{max}. This conclusion is derived in part from the effect of the R ratio on the fatigue crack growth relationships, i.e. as R ratio increases the ΔK value at the onset of accelerated crack growth decreases, but K_{max} is nearly invariant (21–23 MPa m$^{1/2}$). This dependence of accelerated cracking on K_{max} coupled with the relationship $\Delta K = (1 - R)K_{max}$ leads to the relative positions of the crack growth rate curves in ΔK space. A governing role for K_{max} in activating hydrogen-assisted cracking is also consistent with the intergranular crack path. The decohesion concept is commonly invoked as the basic physics for hydrogen-assisted intergranular crack growth in both low-strength and high-strength materials [13,14], and mechanics models for decohesion typically presume that local stress drives crack growth [15,16]. Since the decohesion event depends on both the intensity of the stress field and the volume of material subjected to elevated stress [17], it is reasonable to assume that these condtions are more likely satisfied at K_{max}. At lower K material points further from the crack tip that could potentially experience decohesion sustain lower stresses [18]. It is well known that stress alone does not dictate decohesion-based crack extension, rather it is the stress acting over a microstructure-related characteristic distance [19].

Each da/dN vs. ΔK relationship for X52 line pipe steel in the mixed $H_2 + O_2$ gases at $R = 0.1$ (Fig. 6) exhibited an abrupt acceleration in fatigue crack growth rates that resembles the behavior in high-purity hydrogen gas. In addition, at the acceleration point the crack path was intergranular in the $H_2 + 10$ v.p.p.m. O_2 and $H_2 + 100$ v.p.p.m. O_2 gases. Given such consistencies in characteristics of the da/dN vs. ΔK relationships and crack paths it is reasonable to surmise that K_{max} governs the onset of hydrogen-accelerated crack growth in the mixed gases as well. However, this supposition can be explored by following the approach of Suresh and Ritchie, i.e. examining fatigue crack growth relationships as a function of the ratio R. In high-purity hydrogen the fatigue crack growth rate curves had the expected relative positions in ΔK space given the relationship $\Delta K = (1 - R)K_{max}$ and a constant value of K_{max} to trigger accelerated crack growth (Fig. 2), but the behavior in the mixed gas was dramatically different. As shown in Fig. 6 for the $H_2 + 1000$ v.p.p.m. O_2 gas, crack growth rates accelerated at $\Delta K = 17$ MPa m$^{1/2}$ ($K_{max} = 19$ MPa m$^{1/2}$) for $R = 0.1$, but when the R ratio was increased to 0.5 the da/dN vs. ΔK relationship remained coincident with the relationship in air up to the maximum ΔK applied during the test ($\Delta K = 29$ MPa m$^{1/2}$ and $K_{max} = 57$ MPa m$^{1/2}$). These results suggest that the onset of accelerated crack growth in the $H_2 + O_2$ gases is not solely dictated by K_{max}.

Since K_{max} alone does not govern the onset of accelerated crack growth in the mixed $H_2 + O_2$ gases a prominent role for other mechanical variables must be considered. Conceptually, oxygen in the mixed gas effectively passivates the steel surface and impedes the ingress of atomic hydrogen [4]. However, based on stress–corrosion cracking models [20–26] crack tip passivation is a transient state, since the passive surface layer can be mechanically destabilized (ruptured) by deformation. Exposure of base material to the crack growth accelerating environmental species is then determined by competition between the rate of bare surface creation and the rate of repassivation. Conventionally the mechanical variable that dictates the rate of bare surface creation is the crack tip strain rate [22–25]. Specifically, the time between rupture events (t_{rup}) is estimated from the ratio of surface layer rupture strain to crack tip strain rate [22,23,26]. As t_{rup} decreases with increasing strain rate the extent of repassivation decreases, enabling access of the crack growth accelerating environmental species to the base material.

A variation of the interaction between crack tip deformation and passivation described above is invoked to formulate a physical model for hydrogen-accelerated fatigue crack growth of X52 steel in mixed $H_2 + O_2$ gases. In this alternative model the rate of bare surface creation does not explicitly result from the continuum strain rate-driven rupture of the passive surface layer. Rather, the mechanism for creating bare crack tip surface is related to an idealized fatigue crack extension process in inert environments, i.e. crack tip blunting on the loading segment followed by resharpening on unloading [27,28]. As the loading segment proceeds the sharp crack effectively extends via crack tip

Please cite this article in press as: Somerday BP et al. Elucidating the variables affecting accelerated fatigue crack growth of steels in hydrogen gas with low oxygen concentrations. Acta Mater (2013), http://dx.doi.org/10.1016/j.actamat.2013.07.001

blunting, creating a new reactive surface that is exposed to the $H_2 + O_2$ gas. Oxygen can be adsorbed on this new crack tip surface to create a passive layer, and it is assumed that the passive layer is continuously formed during the loading–unloading cycle. At the onset of the subsequent loading segment this passive layer on the sharp crack tip then essentially ruptures immediately as the crack extends via blunting. Thus, with reference to the conventional stress–corrosion cracking models, the time between rupture events t_{rup} is the load cycle period, i.e. $1/f$. In the current model the extent of repassivation is quantified as the amount of oxygen that adsorbs on the new blunted crack tip surface during the load cycle period. The viability of key mechanistic assumptions in this model are critically examined below.

Based on these concepts the following scenario is proposed for fatigue crack growth of X52 steel in mixed $H_2 + O_2$ gases. Under constant load amplitude (i.e. increasing ΔK) testing the first interval of fatigue crack growth was characterized by the idealized blunting and resharpening mechanism, in which rates follow the conventional relationship $da/dN = A(\Delta K)^m$ expected in inert environments. The rate of new crack tip surface creation per unit time is proportional to this inert environment crack growth increment per cycle multiplied by the load cycle frequency, i.e. $(da/dN)f$. As crack extension progresses under rising ΔK, da/dN increases and the rate of new surface creation increases concomitantly. Alternatively, under constant ΔK testing, in which the inert environment value of da/dN is invariant, the rate of new crack tip surface creation can be increased by raising f. In either case oxygen coverage of the freshly exposed crack tip is dictated by the balance between the rate of new surface creation and the rate of oxygen adsorption. For crack growth rates $(da/dN)f$ less than a threshold value the rate of new surface creation is dominated by the rate of oxygen adsorption, and the crack tip becomes fully passivated. However, as the crack growth increment (or frequency) increases the new crack tip surface created during each load cycle cannot be fully passivated. These latter conditions promote atomic hydrogen ingress from the crack tip surface, enabling activation of hydrogen-accelerated fatigue crack growth. This physical model is consistent with that proposed by Stewart [29] to rationalize the effects of oxygen on hydrogen gas-assisted fatigue crack growth for steels.

The notion that a threshold level of inert environment crack growth rate is necessary to trigger hydrogen-accelerated fatigue crack growth can be tested by establishing a quantitative model. The detailed model development, described in the Appendix, is based on the following assumptions: (1) the area of new crack tip surface created during each load cycle is proportional to the inert environment crack growth increment per cycle da/dN; (2) the extent of oxygen adsorption (i.e. passivation) on the crack tip surface is controlled by the amount of oxygen transported by diffusion without convection through the hydrogen gas filled crack channel during the time $(1/f)$ for one load cycle; (3) when the balance between new surface creation and oxygen transport leads to oxygen coverage below a critical level during the load cycle hydrogen uptake at the crack tip is enhanced and hydrogen-accelerated fatigue crack growth can proceed. The second assumption is based on the expectation that dissociative chemisorption of oxygen on iron is very rapid, so that the rate-limiting step for oxygen adsorption is mass transport to the crack tip. In addition, convection is neglected because of the very small Reynolds number of hydrogen gas (see Appendix).

The essence of the model described in the Appendix is that the crack initially advances by idealized inert environment fatigue mechanisms in each load cycle (i.e. alternating crack tip blunting and resharpening [27,28]), and these crack growth increments are equal to the measured da/dN. At maximum load in each cycle the crack tip surface is assumed to have a semicircular profile, in which the radius is equal to the crack growth increment (Δa). The amount of oxygen adsorbed on this new crack tip surface during the time to reach maximum load is given by a simple mass balance: the adsorbed oxygen is equal to the flux of oxygen through the crack channel to the crack tip. In the most basic model formulation the height of the crack channel is constant and equal to the crack tip opening displacement at maximum load, which is calculated from K_{max} through the classical elastic–plastic fracture mechanics relationship. Based on this framework, as well as additional assumptions and relationships described in the Appendix, an analytical expression is derived that predicts the critical inert environment crack growth rate $(da/dN)f$ required to limit the oxygen surface coverage below the level for passivation $z_{pass}\theta_O$:

$$\left.\frac{da}{dN} f\right|_{crit} = \frac{0.3\chi D p_{tot}(1-\nu^2)}{\pi z_{pass}\theta_O R_g T E \sigma_0}\left(\frac{\Delta K}{\sqrt{a^*}(1-R)}\right)^2 \quad (1)$$

In this expression D is the diffusivity of oxygen in the hydrogen "matrix", p_{tot} and χ are the total pressure and oxygen concentration, respectively, of the bulk gas, z_{pass} and θ_O are the number of oxygen layers required to passivate the surface and density of oxygen atoms in a dense packed FeO layer, respectively, R_g and T are the gas constant and absolute temperature, respectively, ν, E, and σ_0 are Poisson's ratio, elastic modulus, and yield strength, respectively, a^* is the crack length extending from the pre-crack starter notch, and ΔK and R are the stress intensity factor range and load ratio, respectively. Values for D and the ratio $\Delta K/\sqrt{a^*}$ that are relevant to the fatigue crack growth tests on X52 in the mixed $H_2 + O_2$ gases are described in the Appendix.

Eq. (1) can be employed to predict the inert environment crack growth rate required to limit crack tip oxygen surface coverage, i.e. promote hydrogen uptake, which is a minimum condition for hydrogen-accelerated fatigue crack growth. Eq. (1) shows that the critical da/dN value depends on variables such as the oxygen concentration in hydrogen gas, load cycle frequency, and R ratio. When the inert environment da/dN value is fixed the terms in Eq. (1) can be

Please cite this article in press as: Somerday BP et al. Elucidating the variables affecting accelerated fatigue crack growth of steels in hydrogen gas with low oxygen concentrations. Acta Mater (2013), http://dx.doi.org/10.1016/j.actamat.2013.07.001

rearranged so that critical levels for other variables to activate hydrogen-accelerated crack growth can be predicted. For example, the critical load cycle frequency to activate hydrogen-accelerated crack growth can be calculated at a given value of inert environment *da/dN*. Such predictions of critical levels for *da/dN* and *f* as a function of the parameters (e.g. oxygen concentration and *R* ratio) varied during the fatigue crack growth tests on X52 steel are detailed in the Appendix. In the following sections these predictions are compared with the experimental results (Fig. 10a and b), which allows assessment of the model and enables further interpretation of the variables governing accelerated fatigue crack growth in mixed $H_2 + O_2$ gases. These sections are organized by sub-sets of the fatigue crack growth test conditions, emphasizing the bulk gas oxygen concentration χ and the ratio *R*.

4.1. χ = 10 and 100 v.p.p.m., R = 0.1

As discussed in the Appendix, the number of oxygen layers representing a passivated crack tip z_{pass} cannot be independently determined. This parameter was thus calculated from Eq. (1) using data for the increasing ΔK (i.e. constant load amplitude) fatigue crack growth experiment with $\chi = 100$ v.p.p.m. and $R = 0.1$ (FCG18 in Table 3). In this experiment the transition to hydrogen-accelerated crack growth occurred at an inert environment *da/dN* value of 1.0×10^{-5} mm cycle^{-1} (Figs. 6 and 10a), yielding a value of $z_{pass} = 6$ from Eq. (1). Once the value of $z_{pass} = 6$ was established the critical *da/dN* value to activate hydrogen-accelerated crack growth was calculated for the rising ΔK fatigue crack growth experiment with $\chi = 10$ v.p.p.m. and $R = 0.1$. As shown in Fig. 10a, the predicted critical *da/dN* value correlates reasonably well with the extrapolated intersection of the measured *da/dN* vs. ΔK curves in $H_2 + 10$ v.p.p.m. O_2 gas and air, i.e. the onset of hydrogen-accelerated fatigue crack growth. This favorable comparison demonstrates that Eq. (1) captures the quantitative relationship between inert environment *da/dN* and oxygen concentration.

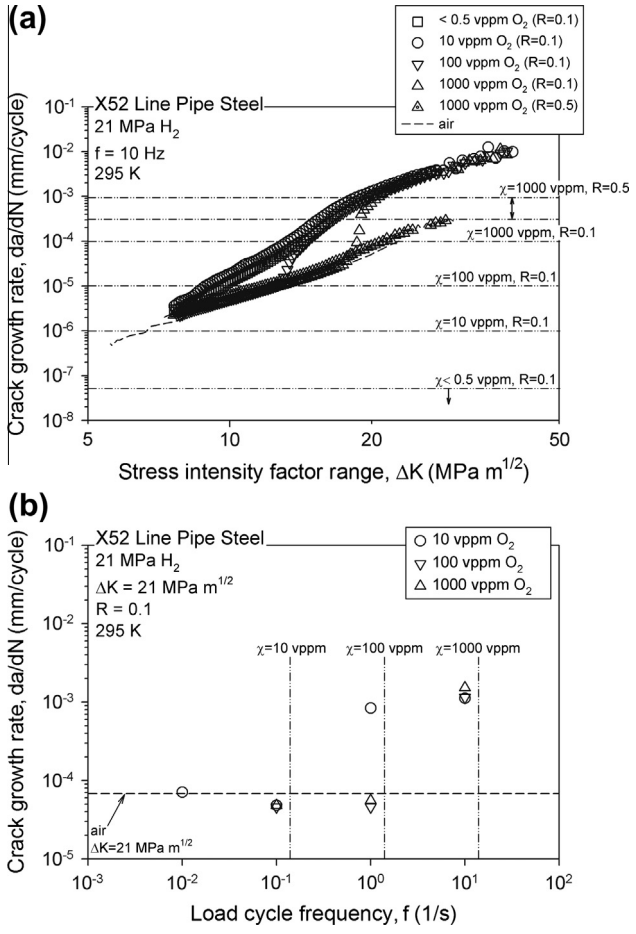

Fig. 10. Comparison between model predictions (dashed-dotted lines) and experimental data (symbols) for (a) increasing ΔK fatigue crack growth tests and (b) constant ΔK fatigue crack growth tests. The *da/dN* vs. ΔK and *da/dN* vs. *f* experimental data are from Figs. 6 and 9, respectively. Values for the model predictions are from Tables A1 and A2.

The predictive capability of Eq. (1) was further evaluated by calculating critical values of load cycle frequency *f* to activate hydrogen-accelerated crack growth. With $z_{pass} = 6$ critical values of *f* were calculated for the constant ΔK experiments (i.e. constant inert environment *da/dN*) with $\chi = 10$ and 100 v.p.p.m., and these predictions are displayed in Fig. 10b. As shown in Fig. 10b, the predicted critical *f* values are within the observed frequency ranges representing the transition from crack growth rates in air or inert gas to hydrogen-accelerated crack growth for both $\chi = 10$ and 100 v.p.p.m. These results support the quantitative relationship between inert environment *da/dN*, *f*, and oxygen concentration in Eq. (1).

One mechanistic implication of the positive correlation between the model predictions and experimental data for $\chi = 10$ and 100 v.p.p.m. in Fig. 10a and b is that the mechanical variable governing the onset of hydrogen-accelerated cracking is the crack growth rate. The extent of crack tip coverage (passivation) from the mass of oxygen delivered through the crack channel during the load cycle is dictated by the inert environment *da/dN* value, since this variable correlates with the area of new crack tip surface.

4.2. χ < 0.5 v.p.p.m., R = 0.1

Eq. (1) (with $z_{pass} = 6$) was also applied to predict the critical *da/dN* value to activate hydrogen-accelerated crack growth for increasing ΔK fatigue crack growth experiments in high-purity hydrogen gas. As illustrated in Fig. 10a, the predicted critical *da/dN* value is substantially lower than the expected *da/dN* value at the onset of accelerated crack growth in high-purity hydrogen. Since the previous section validated the predictive capability of Eq. (1) this result for high-purity hydrogen appears to highlight another mechanistic implication. Specifically, the interpretation here is that thresholds for two mechanical variables must be exceeded for accelerated crack growth: a threshold level

Please cite this article in press as: Somerday BP et al. Elucidating the variables affecting accelerated fatigue crack growth of steels in hydrogen gas with low oxygen concentrations. Acta Mater (2013), http://dx.doi.org/10.1016/j.actamat.2013.07.001

of inert environment da/dN for reduced crack tip passivity (enhanced hydrogen uptake) and a threshold level of K_{max} to activate embrittlement, e.g. intergranular cracking, ahead of the crack tip. For the high-purity hydrogen case crack tip oxygen coverage is insignificant at relatively low crack growth rates, but embrittlement and accelerated cracking are not actuated until a critical K_{max} value is reached. At this critical K_{max} value the micromechanical condition dictating crack extension is the attainment of a critical stress acting over a microstructure-related characteristic distance, consistent with the framework proposed by Ritchie [19]. Assuming that the crack tip stress field under fatigue loading is approximated by the continuum solution for monotonic loading [18], the stress at the characteristic distance rises as K_{max} increases. The critical stress and associated threshold K_{max} to activate embrittlement likely depend on variables such as the crack tip hydrogen concentration, yield strength, and microstructure. The threshold inert environment da/dN value for enhanced hydrogen uptake is given by Eq. (1).

4.3. χ = 1000 v.p.p.m., R = 0.1

Again assuming $z_{pass} = 6$, the predicted inert environment da/dN value to activate hydrogen-accelerated fatigue crack growth under rising ΔK conditions for $\chi = 1000$ v.p.p.m. and $R = 0.1$ is indicated in Fig. 10a. In this case the measured da/dN value at the onset of hydrogen-accelerated crack growth is less than the predicted critical da/dN value. Since the quantitative relationship between the critical da/dN value and oxygen concentration in Eq. (1) was previously verified this result may reveal another mechanistic insight. One possibility is that the crack tip oxygen coverage required to inhibit hydrogen uptake is different for the fatigue crack growth experiment at $\chi = 1000$ v.p.p.m. and $R = 0.1$. This possibility is prompted by the observation that the crack path at the onset of hydrogen-accelerated crack growth is transgranular for $\chi = 1000$ v.p.p.m. and $R = 0.1$ (Fig. 7c), whereas the initial hydrogen-assisted crack paths at lower oxygen concentrations are intergranular (Figs. 3a and 7a). The notion here is that less hydrogen uptake may be required to induce the transgranular crack path compared with the intergranular one, i.e. z_{pass} may be higher for the transgranular crack path. This could then lead to a lower critical inert environment da/dN value to activate hydrogen-assisted trangranular fatigue crack growth.

Eq. (1) was also applied to predict the critical load cycle frequency to activate hydrogen-accelerated crack growth under constant ΔK for $\chi = 1000$ v.p.p.m. and $R = 0.1$. As demonstrated in Fig. 10b, the model prediction is higher than the observed frequency range representing the transition from crack growth rates in air or inert gas to hydrogen-accelerated crack growth. The previous speculative arguments pertaining to the relationship between hydrogen-assisted crack path and z_{pass} are presumed to apply to this case as well.

4.4. χ = 1000 v.p.p.m., R = 0.5

The final comparison between model and experiment is for the rising ΔK fatigue crack growth test with $\chi = 1000$ v.p.p.m. and $R = 0.5$. Figs. 6 and 10a show that hydrogen-accelerated crack growth is not observed for the experiment at $\chi = 1000$ v.p.p.m. and $R = 0.5$, i.e. crack growth rates in the mixed $H_2 + O_2$ gas are coincident with those in air up to the highest applied ΔK level. Consistent with the experiment, Eq. (1) (for $z_{pass} = 6$) accurately predicts that the critical da/dN value for hydrogen-accelerated crack growth is beyond the final point in the measured dataset. (The predicted critical da/dN value in Fig. 10a is displayed as a range, as explained in the Appendix.) Given the agreement between model and experiment the implicit physical insight into this behavior is that the height of the crack channel increases at higher R ratios, augmenting the flux of oxygen to the crack tip. Hydrogen-accelerated crack growth can only be triggered when this enhanced mass transport and attendant oxygen adsorption is sufficiently offset by the creation of new crack tip surface area, i.e. at higher crack growth rates. According to Wei [30] such an effect of the R ratio confirms that the rate-limiting step in gaseous environment-assisted fatigue crack growth is mass transport through the crack channel and not crack tip surface reactions.

Collectively, the comparisons between model and experiment just presented give credence to the physical model embodied by Eq. (1) (e.g. the rate balance between new crack tip surface creation and diffusion-limited oxygen adsorption) and its predictive capability. In addition, these comparisons demonstrate that the onset of accelerated fatigue crack growth in mixed $H_2 + O_2$ gases is likely governed by both K_{max} and the inert environment crack growth rate.

Although the favorable comparison between model and experiment provides confidence in the physical model, two key assumptions are critically examined here. The first assumption is that the mechanism for rupture of the passive layer and creating bare crack tip surface area is related to repetitive crack tip blunting and resharpening during fatigue crack growth. As discussed earlier, an alternative view advocated by the stress–corrosion cracking community is that rupture of the passive layer and concomitant creation of bare crack tip surface area are driven by the continuum crack tip strain rate [22–26]. At issue is whether modifying the model expression in Eq. (1) to reflect the crack tip strain rate mechanism leads to an improved correlation between predictions and experimental data. In the current model expression (Eq. (1)) the rate of surface area creation is quantified by the term $(da/dN)f$. An alternative term based on the crack tip strain rate mechanism can be formulated by assuming the strain rate ($\dot{\varepsilon}_{ct}$) is related to ΔK through the relationship $\dot{\varepsilon}_{ct} = \beta \Delta K^{\lambda} f$, in which β and λ are material constants [26,31]. When the local continuum strain reaches a critical level and ruptures the passive layer the exposed crack tip area can be assumed to be proportional to the cyclic crack tip opening displacement

Please cite this article in press as: Somerday BP et al. Elucidating the variables affecting accelerated fatigue crack growth of steels in hydrogen gas with low oxygen concentrations. Acta Mater (2013), http://dx.doi.org/10.1016/j.actamat.2013.07.001

(ΔCTOD), which is related to ΔK through the relationship $\Delta CTOD = \Delta K^2/2E\sigma_0$ [27,28]. The rate of surface area creation then rationally scales as the product of the crack tip strain rate and the crack tip area, yielding the quantity $\beta f(\Delta K^{\lambda}\Delta K^2)/2E\sigma_0$. Since measurements of deformation on the free surface ahead of fatigue crack tips in steel imply that λ is approximately equal to 2 [32], the rate of surface area creation at the crack tip is proportional to $(\Delta K^4)f$. Considering the crack tip blunting and resharpening model, the bare surface creation rate $(da/dN)f$ can be recast in terms of ΔK through the relationship $da/dN = A\Delta K^m$, i.e. $(da/dN)f = (A\Delta K^m)f$, in which m is approximately equal to 4 based on the da/dN vs. ΔK relationships for air and inert gas in Fig. 2. The preceding analysis suggests that the bare surface creation rate term in Eq. (1) may depend on $(\Delta K^4)f$ for either presumed mechanism. Thus, since Eq. (1) includes a fitting parameter (the number of oxygen layers required to passivate the surface z_{pass}), it is unlikely that comparing predictions from the two model variants to fatigue crack growth data for X52 in mixed $H_2 + O_2$ gases can provide a definitive insight into the operative bare surface creation mechanism.

The other feature of the physical model that must be examined is the assumption that the crack advances by an increment Δa each cycle, which is an inherent characteristic of the fatigue crack growth mechanism based on alternating crack tip blunting and resharpening. According to Ritchie [28] the blunting–resharpening mechanism provides a first order description of fatigue crack growth rate behavior in the mid-range of growth rates (approximately 10^{-6}–10^{-4} mm cycle^{-1}). However, as fatigue crack growth rates approach the near threshold regime crack growth becomes increasingly intermittent, i.e. the crack remains stationary for an accumulated number of cycles ΔN, then extends by an increment Δa in the following cycle [33]. Thus in the near threshold regime the actual Δa increments associated with specific ΔK values may exceed the characteristic da/dN levels quantified in the fatigue crack growth experiment. Reviewing the development of the physical model in the Appendix intermittent crack extension does not compromise the model, since oxygen coverage (passivation) of new crack tip surface is still dictated by the balance between crack growth rate $(\Delta a)f$ and oxygen adsorption rate during the cycle in which the crack extends. The possible ambiguity is not the physical foundation of the model, but comparing model predictions with experimental data. For example, due to possible intermittent crack extension the Δa increments associated with specific ΔK values may be greater than the respective da/dN values measured during the experiments. Furthermore, in principle Fig. 10a compares the predicted critical Δa value required to preclude crack tip passivation, i.e. activate hydrogen-accelerated fatigue crack growth, with measured da/dN. Consequently, the predicted critical Δa value may progressively exceed the measured da/dN value at the onset of hydrogen-accelerated fatigue crack growth as ΔK decreases and intermittent crack growth becomes more predominant. This trend is not observed in Fig. 10a, suggesting that measured da/dN values in the lower range of ΔK do not reflect significant intermittent crack extension.

5. Conclusions

Fatigue crack growth relationships da/dN vs. ΔK were measured for X52 line pipe steel in high-purity hydrogen gas and mixed $H_2 + O_2$ gases containing up to 1000 v.p.p.m. oxygen. The following conclusions can be derived from this study.

- In both high-purity hydrogen gas and mixed $H_2 + O_2$ gases fatigue crack growth rates were initially coincident with those measured in air or inert gas, but as the crack extended under increasing ΔK these rates abruptly accelerated. The ΔK value at the onset of accelerated crack growth systematically increased as the hydrogen gas was enriched with oxygen.
- The onset of accelerated crack growth was associated with hydrogen-induced intergranular cracking in high-purity hydrogen as well as mixed $H_2 + O_2$ gases with 10 and 100 v.p.p.m. oxygen. In the H_2 + 1000 v.p.p.m. O_2 gas hydrogen-accelerated cracking adopts a transgranular mode for all ΔK levels.
- In addition to the bulk gas oxygen concentration, the onset of hydrogen-accelerated crack growth is affected by the load cycle frequency and load ratio R. Either a lower load cycle frequency or a higher R ratio delay the onset of hydrogen-accelerated crack growth to higher ΔK levels.
- Hydrogen-accelerated fatigue crack growth is actuated when threshold levels of both inert environment crack growth rate and K_{max} are exceeded. The inert environment crack growth rate dictates hydrogen uptake through its effect on the extent of crack tip oxygen coverage (i.e. passivation), while K_{max} governs the activation of hydrogen-assisted fracture modes through its relationship to the crack tip stress field.
- The relationship between inert environment crack growth rate and crack tip hydrogen uptake was established through the development of an analytical model. The model expression was formulated based on the assumption that crack tip oxygen coverage can be quantified by considering the rate balance between creation of new crack tip surface area and diffusion-limited oxygen transport through the crack channel to this surface. Provided that K_{max} exceeds the threshold value to activate stress-driven hydrogen embrittlement this model illustrates that stimulation of hydrogen-accelerated crack growth depends on the interplay between the inert environment crack growth increment per cycle, load cycle frequency, R ratio, and bulk gas oxygen concentration.

Please cite this article in press as: Somerday BP et al. Elucidating the variables affecting accelerated fatigue crack growth of steels in hydrogen gas with low oxygen concentrations. Acta Mater (2013), http://dx.doi.org/10.1016/j.actamat.2013.07.001

Acknowledgements

The assistance of Ken Lee in conducting the fatigue crack growth tests in hydrogen gas environments as well as Andy Gardea and Ryan Nishimoto in performing metallography and microscopy is gratefully acknowledged. Sandia National Laboratories is a multi-program laboratory managed and operated by Sandia Corp., a wholly owned subsidiary of Lockheed Martin Corp., for the US Department of Energy's National Nuclear Security Administration under Contract DE-AC04-94AL85000. The experimental work presented here was supported by the US Department of Energy Fuel Cell Technologies Office through the Hydrogen Delivery sub-program element. P.S. gratefully acknowledges support from the US Department of Energy through Grant GO15045. In addition, B.P.S., P.S., and R.K. acknowledge support from the International Institute for Carbon Neutral Energy Research, sponsored by the World Premier International Research Center Initiative, MEXT, Japan.

Appendix A

In this appendix models are established that predict the threshold level of inert environment fatigue crack growth rate necessary to preclude crack tip passivation, enabling hydrogen-accelerated crack growth in mixed $H_2 + O_2$ environments. Analytical model expressions are developed from the mechanical, kinetic, and thermodynamic relationships associated with the following presumed physical model: (1) as load increases in each cycle the crack tip is blunted to a semicircular profile, representing an increment in inert environment fatigue crack growth Δa; (2) crack tip blunting (i.e. crack extension) creates new surface area, and oxygen out-competes hydrogen for these freshly exposed reactive adsorption sites; (3) dissociative chemisorption of oxygen on iron is very rapid, so that the rate-limiting step for oxygen adsorption is mass transport to the crack tip; (4) the mass transport kinetics are described by oxygen diffusion through the hydrogen gas "matrix" in the crack channel; (5) the extent of oxygen adsorption on the crack tip surface is dictated by the balance between rates of new surface creation and oxygen transport; (6) when the rate of new crack tip surface creation, i.e. $(da/dN)f$, reaches a critical level the extent of oxygen coverage decreases below the level required to passivate the surface. Once the latter condition is attained hydrogen uptake at the crack tip is enhanced and hydrogen-accelerated fatigue crack growth can proceed. In the following sections analytical model expressions for the critical inert environment $(da/dN)f$ required to preclude crack tip passivation, i.e. activate hydrogen-accelerated fatigue crack growth, are developed for two limiting cases: (1) the height of the oxygen transport channel is constant and equal to the crack tip opening displacement at maximum load; (2) the height of the oxygen transport channel is a function of the time-varying load, which modifies the oxygen concentration profile in the channel by inducing lamellar flow. The degree of reality in these cases may be substantiated by their ability to interpret experimental results.

A.1. Model based on constant crack opening

For the following analysis of oxygen diffusion through a hydrogen gas filled crack channel with constant height an idealized crack geometry is invoked, as shown in Fig. A1. For the compact tension specimens used in the fatigue crack growth experiments the total crack length a includes the length of the pre-crack starter notch, whereas a^* is the length of the crack extending from the notch root, i.e. the pre-crack plus crack extension in the hydrogen environment. Consistent with the crack geometry proposed by Wei to model mass transport of hydrogen to a crack tip [30,34], the crack channel consists of parallel surfaces separated by a distance h, in which h is set as the crack tip opening displacement (CTOD) at maximum load. (The assumption of constant h for this case effectively means that the load rises from its minimum to maximum value instantaneously, i.e. a square loading waveform.) One consequence of not considering dynamic crack opening is that the analysis ignores possible gas flow in and out of the crack channel, with corresponding changes in the oxygen concentration profile. In addition, without gas leaving or entering the crack channel by either laminar or turbulent flow variations in h lead to a corresponding variation in the total gas pressure p_{tot}, however, a potential change in p_{tot} has no effect on the critical crack growth rate $(da/dN)f$, as shown in the following analysis. Consequences regarding laminar flow associated with dynamic crack opening are discussed in the last section of this Appendix.

The essence of the model development is to formulate a mass balance between oxygen adsorbed on new crack tip surface and oxygen transported through the crack channel during a load cycle. As detailed in Section 4, new crack tip

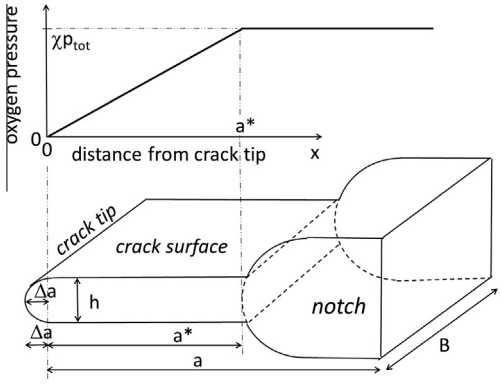

Fig. A1. (Bottom) Idealized crack geometry with the hemi-cylindrical crack tip, hemi-cylindrical pre-crack starter notch, and parallel crack surfaces. (Top) The assumed oxygen partial pressure profile with an infinite oxygen supply from the notch volume and an oxygen sink at the crack tip due to new surface creation from the crack growth increment Δa.

Please cite this article in press as: Somerday BP et al. Elucidating the variables affecting accelerated fatigue crack growth of steels in hydrogen gas with low oxygen concentrations. Acta Mater (2013), http://dx.doi.org/10.1016/j.actamat.2013.07.001

surface is created through inert environment crack extension, which is idealized by the crack tip blunting and resharpening mechanism [27,28]. In one load cycle the crack extends within the time Δt by an increment Δa, which corresponds to an inert environment crack growth rate of $\Delta a/\Delta t = (\Delta a)f$, where f is the load cycle frequency. Based on the assumed semicircular crack tip profile at maximum load (Fig. A1), the crack growth increment produces a new bare surface area equal to $\pi(\Delta a)B$. Oxygen will be preferentially adsorbed compared with hydrogen on this new bare surface. This assumption is justified by the much larger negative formation energy of iron oxide in comparison with iron hydride.

The crack tip surface acts as a sink for oxygen, and the amount of oxygen adsorbed on the surface during time Δt is denoted Δn_O. The corresponding depletion of oxygen in the near crack tip gas is counteracted by oxygen diffusion from the notch volume (oxygen source). After a characteristic time t_d, defined as

$$t_d = \frac{(a^*)^2}{\pi^2 D} \tag{A1}$$

where D is the diffusion coefficient of oxygen in hydrogen, a steady-state oxygen concentration profile is established within the crack channel of length a^*. Coupling the interdiffusion coefficient for oxygen and hydrogen at 0.1 MPa ($D = 7.6 \times 10^{-5}\ \mathrm{m^2\ s^{-1}}$ [35,36]) and the reciprocal dependence between D and the total pressure p_{tot} for ideal gases yields the relationship [35,36]:

$$D\ (\mathrm{m^2\ s^{-1}}) = \frac{7.6 \times 10^{-6}}{p_{tot}\ (\mathrm{MPa})} \tag{A2}$$

For the fatigue crack growth experiments in the current study the maximum crack length preceding hydrogen-accelerated fatigue crack growth a^* and total gas pressure were 13 mm and 21 MPa, respectively. Based on these inputs, Eqs. (A1) and (A2) yield $t_d = 47$ s, which is a very short characteristic time compared with the duration of the experiments (tens of hours). Therefore, a steady-state oxygen concentration profile having a constant gradient is established between the notch root at $x = a^*$ and the crack tip at $x = 0$. (Strictly, the profile is quasi-stationary because a^* is increasing slowly with time.)

The steady-state diffusion flux of oxygen in the crack channel is given by Fick's First Law:

$$J = D\frac{n(a^*) - n(0)}{a^*} \tag{A3}$$

where $n(x)$ is the oxygen concentration at x obtained from the ideal gas law in units of mole per volume

$$n(x) = \frac{p(x)}{R_g T} \tag{A4}$$

where p is the partial pressure of oxygen, T is the absolute temperature, and R_g is the gas constant. At the notch root ($x = a^*$) the oxygen concentration should be equal to that in the bulk gas, i.e.

$$n(a^*) = \frac{\chi p_{tot}}{R_g T} \tag{A5}$$

in which χ is the volume fraction of oxygen in the hydrogen gas. Based on the assumption that the rate of oxygen adsorption on the crack tip surface is given by the rate of oxygen transport, the maximum amount of oxygen adsorbed in the time increment Δt is equal to the mass of oxygen supplied by the stationary flux J through the crack channel area hB according to Eq. (A3) and Fig. A1:

$$\Delta n_{Omax} = JhB\Delta t = D\frac{n(a^*) - n(0)}{a^*}hB\Delta t \tag{A6}$$

It has been tacitly assumed that oxygen is transported through the crack channel by diffusion from the notch root only, neglecting contributions from both sides of the crack, i.e. one-dimensional diffusion. This assumption appears to be reasonable for $a^* < B$, as applicable for typical crack lengths preceding the onset of hydrogen-accelerated crack growth in the experiments.

The actual oxygen concentration at the crack tip, $n(0)$, is determined by the efficiency of the bare crack tip surface as an oxygen sink. For simplicity we assume an infinite sink efficiency, i.e. $n(0) = 0$. This appears to be reasonable, because at the lowest oxygen concentration of ~1 v.p.p.m. in 21 MPa hydrogen gas the oxygen partial pressure is 21 Pa. At this pressure and for a sticking coefficient of unity kinetic gas theory implies that about 10^4 monolayers are adsorbed in 1 s. For the highest load cycle frequency of 10 Hz this corresponds to 10^3 monolayers during one cycle. The infinite sink assumption then leads to the simplified relationship:

$$\Delta n_{Omax} = D\frac{n(a^*)}{a^*}hB\Delta t \tag{A7}$$

Now it is assumed that a certain quantity of adsorbed oxygen is required during one load cycle to passivate a crack tip surface having the area $\pi(\Delta a)B$. This quantity should correspond to a surface coverage $\theta_{pass} = z_{pass}\theta_O$, where z is the number of dense packed oxygen layers in the passivating FeO surface film and θ_O is the density of oxygen moles in a close packed layer. Expressed in terms of the surface coverage, the number of oxygen moles required for passivation per load cycle is:

$$\Delta n_{pass} = z_{pass}\theta_O B\pi\Delta a \tag{A8}$$

Here passivation refers to an oxygen layer of certain thickness which inhibits hydrogen uptake and concomitant crack growth acceleration. Thus, if crack channel diffusion does not supply an oxygen quantity equal to Δn_{pass} the crack growth rate starts to accelerate toward the characteristic rate in pure hydrogen. This occurs when $\Delta n_{Omax} \leqslant \Delta n_{pass}$, leading to the following expression derived from Eqs. (A7) and (A8):

$$D\frac{n(a^*)}{a^*}hB\Delta t \leqslant z_{pass}\theta_O B\pi\Delta a \tag{A9}$$

Please cite this article in press as: Somerday BP et al. Elucidating the variables affecting accelerated fatigue crack growth of steels in hydrogen gas with low oxygen concentrations. Acta Mater (2013), http://dx.doi.org/10.1016/j.actamat.2013.07.001

The corresponding critical inert environment crack growth rate required to maintain crack tip oxygen coverage below the level for passivation, i.e. the crack growth rate for activating hydrogen-accelerated fatigue crack growth, then becomes:

$$\left.\frac{\Delta a}{\Delta t}\right|_{crit} = D\frac{n(a^*)}{\pi a^* z_{pass}\theta_O}h \tag{A10}$$

Following the environmental fatigue crack growth modeling by Wei [30,34] it is assumed that hydrogen-accelerated crack growth occurs at the maximum load point, so that the effective timeframe for oxygen passivation is half the load cycle or $1/2f$. Inserting Eq. (A5) and $\Delta t = 1/2f$ into Eq. (A10) yields the expression:

$$(\Delta a)f|_{crit} = D\frac{\chi p_{tot}}{2\pi a^* z_{pass}\theta_O R_g T}h \tag{A11}$$

In the kinetic theory of ideal gases the diffusion coefficient is inversely proportional to the pressure, and therefore the product Dp_{tot} is independent of the total pressure.

The crack channel height (or crack tip opening displacement) h, corresponding to the maximum stress intensity factor K_{max}, is approximated by the elastic–plastic solution for the CTOD under monotonic loading [18], e.g.

$$h = 0.6(1-\nu^2)\frac{\sigma_0}{E}\left(\frac{K_{max}}{\sigma_0}\right)^2 \tag{A12}$$

where σ_0 is the yield strength, E is the elastic modulus, and ν is the Poisson's ratio. Then Eq. (A11) becomes:

$$(\Delta a)f|_{crit} = \frac{\chi Dp_{tot}}{2\pi a^* z_{pass}\theta_O R_g T}0.6(1-\nu^2)\frac{\sigma_0}{E}\left(\frac{K_{max}}{\sigma_0}\right)^2 \tag{A13}$$

Rearranging Eq. (A13) and introducing the relationship $K_{max} = \Delta K/(1-R)$ gives:

$$(\Delta a)f|_{crit} = \frac{0.3\chi Dp_{tot}(1-\nu^2)}{\pi z_{pass}\theta_O R_g T E\sigma_0}\left(\frac{\Delta K}{\sqrt{a^*}(1-R)}\right)^2 \tag{A14}$$

For later convenience the ratio $\Delta K/\sqrt{a^*}$ is represented by the parameter C. In addition, the crack growth increment Δa is assumed to represent the characteristic crack growth rate da/dN measured during fatigue crack growth experiments, as implied by the crack tip blunting and resharpening mechanism. These two substitutions lead to the expression:

$$\left.\frac{da}{dN}f\right|_{crit} = \frac{0.3\chi Dp_{tot}(1-\nu^2)}{\pi z_{pass}\theta_O R_g T E\sigma_0}\left(\frac{C}{(1-R)}\right)^2 \tag{A15}$$

The form of Eq. (A15) allows predictions of the critical inert environment crack growth rate required to preclude crack tip passivation, i.e. activate hydrogen-accelerated fatigue crack growth. When applying Eq. (A15) to the range of fatigue crack growth experiments in the current study many of the parameters are invariant. For example:

1. for the X52 steel $\nu = 0.3$, $E = 200$ GPa, and $\sigma_o = 430$ MPa;
2. the thermal energy R_gT is equal to 8.314×295 J mol^{-1} at room temperature;
3. following Eq. (A2) the product of the oxygen diffusion coefficient in hydrogen and the total gas pressure Dp_{tot} is equal to 7.6 Pa m^2 s^{-1};
4. the density of oxygen atoms in a close packed FeO layer θ_O is 1.5×10^{-5} mol m^{-2}.

Inserting these values into Eq. (A15) leads to the simplified form:

$$\left.\frac{da}{dN}f\right|_{crit} = 2.1\times10^{-4}\frac{\chi}{z_{pass}}\left(\frac{C}{(1-R)}\right)^2 \text{ mm cycle}^{-1} \tag{A16}$$

Eq. (A16) provides a prediction for the onset of hydrogen-accelerated crack growth as a function of the inert environment crack growth increment per cycle da/dN, load cycle frequency f, load ratio R, and oxygen concentration in bulk hydrogen gas χ. While these parameters can be readily specified for individual fatigue crack growth tests, C and z_{pass} warrant further consideration.

The parameter $C = \Delta K/\sqrt{a^*}$ is approximately constant for a limited range of crack lengths in the compact tension specimen. For most of the fatigue crack growth tests in this study a^* does not exceed 10 mm. (Recall that a^* is the crack length associated with the oxygen diffusion channel, and its terminal point is defined by the onset of hydrogen-accelerated crack growth.) For a^* up to 10 mm C is approximated by the average value of 150 MPa, which varies less than 20% from the maximum and minimum C values in this crack length interval. Beyond $a^* = 10$ mm C increases monotonically and can reach values as high as 250 MPa at typical final crack lengths. In the current study a^* exceeded 10 mm for only one fatigue crack growth test (FCG21 in Tables 3 and A1), and in this case a^* is defined by the final crack length since hydrogen-accelerated crack growth was not activated.

The number of layers in the passivating film z_{pass} is an unknown quantity. However, this value can be calculated from one test condition then applied to predict the critical inert environment crack growth rate for the other experiments. Considering the constant load amplitude experi-

Table A1
Predicted critical inert environment crack growth rate required to activate hydrogen-accelerated fatigue crack growth for different test conditions of oxygen concentration (χ), load cycle frequency (f), and load ratio (R) according to Eq. (A16) with $z_{pass} = 6$.

Specimen no.	χ (v.p.p.m.)	f (s^{-1})	R	C (MPa)	Critical da/dN (mm cycle^{-1})
FCG9	<0.5	10	0.1	150	$<4.8\times10^{-8}$
FCG17	10	10	0.1	150	9.7×10^{-7}
FCG18	100	10	0.1	150	1.0×10–5[a]
FCG19	1000	10	0.1	150	9.7×10^{-5}
FCG21	1000	10	0.5	150	3.1×10^{-4}
				250	8.7×10^{-4}

[a] This critical da/dN does not represent a prediction but was set at the experimental value for the purpose of calculating z_{pass}.

Please cite this article in press as: Somerday BP et al. Elucidating the variables affecting accelerated fatigue crack growth of steels in hydrogen gas with low oxygen concentrations. Acta Mater (2013), http://dx.doi.org/10.1016/j.actamat.2013.07.001

ment having $R = 0.1$, $f = 10$ Hz, and $\chi = 100$ v.p.p.m. (FCG18 in Tables 3 and A1), the inert environment crack growth increment per cycle da/dN at the transition to hydrogen-accelerated crack growth is 1.0×10^{-5} mm cycle^{-1} (cf. Fig. 6). Inserting these values into Eq. (A16) yields $z_{pass} = 6$, i.e. a coverage of six oxide layers is necessary to passivate the steel crack tip (corresponding to an oxide thickness of about 1 nm, which is somewhat smaller than a natural oxide [37]). Crack tip passivation is quantified by the number of oxygen layers z_{pass}, which is unknown and essentially serves as a fitting parameter. An alternative approach to defining and quantifying the passivation physics is through the parameter $\theta_O S$, in which θ_O is the oxygen surface coverage (mole oxygen per mole adsorption sites) and S is the density of surface adsorption sites (mol m^{-2}) [34]. In this case the condition for passivation is $\theta_O = 1$, and S becomes a fitting parameter.

Once the value of $z_{pass} = 6$ is established as the number of oxide layers required for passivation the predictive capability of Eq. (A16) can be evaluated in several ways. Considering the fatigue crack growth experiments designed to measure da/dN vs. ΔK (Fig. 6) the critical da/dN value precluding crack tip passivation (and activating hydrogen-accelerated fatigue crack growth) can be calculated for combinations of oxygen concentration χ, load cycle frequency f, and load ratio R employed in the tests. These predicted critical da/dN values are summarized in Table A1 for each test and compared with the experimental data in Fig. 10a. Eq. (A16) can also be implemented to predict critical levels of other variables activating hydrogen-accelerated fatigue crack growth, such as the load cycle frequency (Fig. 9). In this case χ, R, and da/dN are specified and the critical f value activating hydrogen-accelerated crack growth is calculated from Eq. (A16). Such predicted critical f levels are summarized for selected tests in Table A2 and compared with experimental data in Fig. 10b.

A.2. Model based on dynamic crack opening

In the following section the above treatment is modified by accounting for the variation in crack channel height h during cyclic loading. Because of the very low dynamic viscosity of hydrogen gas the corresponding changes in gas pressure inside the crack channel are assumed to vanish in a very short time due to hydrogen flowing in or out, leading to an instantaneous equalization of the crack channel pressure with the bulk value in the notch volume. The corresponding flow of hydrogen gas is assumed to be lamellar because of the very low Reynolds number for the given geometry. The Reynolds number is defined as:

$$Re = \frac{\rho v d}{\eta} \tag{A17}$$

where ρ is the mass density of hydrogen (18.9 kg m^{-3} at 21 MPa), η is the dynamic viscosity of hydrogen (8.4×10^{-6} Pa s at 273 K and 0.1 MPa), d is a characteristic length (either crack length or crack opening displacement) with a value between 10^{-4} and 10^{-2} m, and v is the average gas velocity. The latter variable is approximated by the product of crack length ($\sim 10^{-2}$ m) and load cycle frequency ($\leqslant 10$ s^{-1}). Thus the Reynolds number is between 23 and 2300, where the upper bound is close to the critical value 2040 ± 10 given for the onset of turbulent flow in a tube [38]. This estimated Reynolds number for the current problem is further decreased, because the viscosity is increased for pressures above 0.1 MPa. The absence of turbulent flow prohibits mixing of oxygen along the crack length. The situation becomes more complex at the point of minimum crack opening, where possible crack surface asperity contact may trigger turbulence. The consequences are discussed at the end of this Appendix.

For the sake of simplicity turbulent flow is neglected, and the analysis continues with a first order approximation of a simple oxygen partial pressure profile in the channel of a "breathing crack", as shown in Fig. A2. It is assumed that the gas velocity gradient across the crack channel height during lamellar flow as well as diffusion at $a(t)$ do not significantly affect the oxygen profile at $x = 0$. Any turbulent flow would enhance mixing of oxygen perpendicular to the x-direction, supporting the idealized oxygen profile shown in Fig. A2. Along the crack channel in the x-direction turbulence would accelerate mass transport by diffusion, which is not taken into account in the following considerations.

According to the model described in Fig. A2 the position $x = a(t)$, representing the terminal point of the oxygen concentration gradient remaining from minimum crack opening, is defined by the amount of gas flowing into the crack channel as h increases. This gas volume is necessary to adjust the pressure in the crack channel to equal the pressure in the notch volume p_{tot}. This volume balance leads to the expression:

$$[a^* - a(t)]h(t)B = [h(t) - h_l)]a^*B$$

or

$$\frac{a(t)}{a^*} = \frac{h_l}{h(t)} \tag{A18}$$

where B is the width of the crack channel (thickness of the compact tension specimen).

The crack opening (or crack channel height) $h(t)$ varies during one cycle. In the model based on constant crack

Table A2
Predicted critical load cycle frequency required to activate hydrogen-accelerated fatigue crack growth for different test conditions of oxygen concentration (χ), load ratio (R), and inert environment crack growth rate (da/dN) according to Eq. (A16) with $z_{pass} = 6$.

Specimen no.	χ (v.p.p.m.)	R	Inert da/dN (mm cycle^{-1})	C (MPa)	Critical f (s^{-1})
FCG20	10	0.1	7×10^{-5}	150	0.14
FCG20	100	0.1	7×10^{-5}	150	1.4
FCG20	1000	0.1	7×10^{-5}	150	14

Please cite this article in press as: Somerday BP et al. Elucidating the variables affecting accelerated fatigue crack growth of steels in hydrogen gas with low oxygen concentrations. Acta Mater (2013), http://dx.doi.org/10.1016/j.actamat.2013.07.001

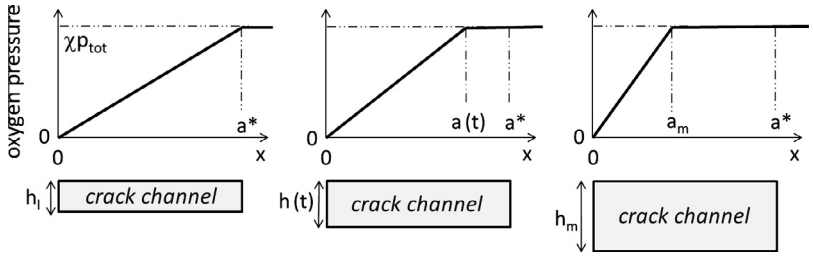

Fig. A2. Assumed oxygen partial pressure profile in a "breathing" crack of length a^*. The crack channel profile shown schematically as a rectangular box varies its opening between minimum (h_l) and maximum (h_m) values. Because of the low viscosity of hydrogen gas the total gas pressure in the crack channel attains the same value as the bulk gas. Expansion and contraction of the oxygen profile between a_m and a^* is due to lamellar flow of the hydrogen gas caused by the imposed changes in the crack channel volume (cf. text).

opening the height of the crack channel was set as the CTOD, in which the relationship between the CTOD and remote loading was determined from elastic–plastic considerations. For this model considering dynamic crack opening it is more convenient to assume that crack opening behaves in a linear elastic fashion. In this case the relationship between crack opening and the stress intensity factor K is linear. In the fatigue crack growth experiments in this study K varied linearly during one crack opening cycle with a period τ, and the corresponding change in h was then assumed to be:

$$h(t) = \begin{cases} h_l + 2(h_m - h_l)t/\tau & \text{for } 0 \leqslant t \leqslant \tau/2 \\ 2h_m - h_l - 2(h_m - h_l)t/\tau & \text{for } \tau/2 < t \leqslant \tau \end{cases} \tag{A19}$$

As a consequence of the oxygen concentration profile and crack channel height varying during one cycle the flux of oxygen towards the crack tip depends on time, and Eq. (A7) becomes:

$$N_{Omax} = \int_0^\tau D\frac{n(a)}{a}hBdt \tag{A20}$$

where the quantity N_{Omax} is the maximum moles of oxygen transported by crack channel diffusion during one cycle. Since $n(a) = n(a^*) = \chi p_{tot}/R_gT$ (see Fig. A2), inserting this quantity as well as Eqs. (A18) and (A19) into Eq. (A20) yields the expression:

$$\begin{aligned} N_{Omax} &= \frac{DB\chi p_{tot}}{R_gT}\int_0^\tau \frac{h^2(t)}{a^* h_l}dt \\ &= \frac{DB\chi p_{tot}}{R_gT}\int_{h_l}^{h_m} \frac{h^2(t)}{a^* h_l}\frac{dt}{dh}dh \\ &= \frac{2DB\chi p_{tot}}{R_gTa^* h_l}\int_{h_l}^{h_m} \frac{h^2(t)\tau}{(h_m - h_l)}dh \\ &= \frac{2\tau}{3}\frac{DB\chi p_{tot}}{R_gTa^* h_l}\left[h_m^2 + h_m h_l + h_l^2\right] \end{aligned} \tag{A21}$$

By defining an average h value using the expression:

$$\bar{h} = \frac{2[h_m^2 + h_m h_l + h_l^2]}{3h_l} \tag{A22}$$

Eq. (A21) then becomes:

$$N_{Omax} = \tau\frac{DB\chi p_{tot}}{R_gTa^*}\bar{h} \tag{A23}$$

When Eq. (A23) is substituted for Eq. (A7) the form of Eq. (A11) is retained, since $\tau = 1/f$. Thus the derivation and discussion following Eq. (A11) remains essentially unchanged. One exception is that Eq. (A12) is superseded by Eq. (A22), in which h_m and h_l depend on K_{max} and K_{min}, respectively. Ultimately the predicted activation of hydrogen-accelerated crack growth for the breathing crack still depends on the inert environment crack growth increment per cycle da/dN, load cycle frequency f, and oxygen concentration χ, following the functional form of Eq. (A16). The dependence on ratio R (K_{min}/K_{max}) must be introduced through relationships between h_m and K_{max} as well as h_l and K_{min} (cf. Eq. (A22)).

The idealized oxygen profile in Fig. A2 may not describe the real profile for low values of h_l where crack surface asperity contact due to surface roughness of the order of h_l may cause considerable turbulence. Such turbulence may result despite the fact that the characteristic length d in the definition of the Reynolds number (Eq. (A17)) scales with h_l, yielding a decreasing Reynolds number that favors lamellar flow. A more rigorous treatment of this condition is beyond the scope of the present study.

References

[1] Suresh S, Ritchie RO. Metal Sci 1982;16:529.
[2] Nelson HG. In: Briant CL, Banerji SK, editors. Treatise on materials science and technology: embrittlement of engineering alloys. New York: Academic Press; 1983. p. 275.
[3] Wei RP, Gangloff RP. In: Wei RP, Gangloff RP, editors. Fracture mechanics: perspectives and directions (twentieth symposium), ASTM STP 1020. West Conshohocken, PA: ASTM; 1989. p. 233.
[4] Holbrook JH, Cialone HJ, Collings EW, Drauglis EJ, Scott PM, Mayfield ME. In: Gangloff RP, Somerday BP, editors. Gaseous hydrogen embrittlement of materials in energy technologies, vol. 2. Cambridge: Woodhead Publishing; 2012. p. 129.
[5] Nelson HG. In: Thompson AW, Bernstein IM, editors. Effect of hydrogen on behavior of materials. Warrendale, PA: The Metallurgical Society of AIME; 1976. p. 602.
[6] Johnson HH. In: Staehle RW, Hochmann J, McCright RD, Slater JE, editors. Stress corrosion cracking and hydrogen embrittlement of iron based alloys. Houston, TX: NACE; 1977. p. 382.

Please cite this article in press as: Somerday BP et al. Elucidating the variables affecting accelerated fatigue crack growth of steels in hydrogen gas with low oxygen concentrations. Acta Mater (2013), http://dx.doi.org/10.1016/j.actamat.2013.07.001

[7] Frandsen JD, Marcus HL. Metall Trans A 1977;8A:265.
[8] Cialone HJ, Holbrook JH. In: Raymond L, editor. Hydrogen embrittlement: prevention and control. West Conshohocken, PA: ASTM; 1988. p. 134.
[9] Fukuyama S, Yokogawa K, Araki M. In: Cengdian L, Nichols RW, editors. Pressure vessel technology, vol. 2. Oxford: Pergamon Press; 1988. p. 1181.
[10] Fukuyama S, Yokogawa K. Pressure vessel technology, vol. 2. Essen: Verband der Technischen Uberwachungs-Vereine; 1992. p. 914.
[11] ASTM E647-05. Annual book of ASTM standards. West Conshohocken, PA: ASTM.
[12] Cialone HJ, Holbrook JH. Metall Trans A 1985;16A:115.
[13] McMahon CJ. Eng Fract Mech 2001;68:773.
[14] Martin ML, Somerday BP, Ritchie RO, Sofronis P, Robertson IM. Acta Mater 2012;60:2739.
[15] Akhurst KN, Baker TJ. Metall Trans A 1980;12A:1059.
[16] Gerberich W. In: Gangloff RP, Somerday BP, editors. Gaseous hydrogen embrittlement of materials in energy technologies, vol. 2. Cambridge: Woodhead Publishing; 2012. p. 209.
[17] Novak P, Yuan R, Somerday BP, Sofronis P, Ritchie RO. J Mech Phys Solids; 58:206.
[18] McMeeking RM. J Mech Phys Solids 1977;25:357.
[19] Ritchie RO, Knott JF, Rice JR. J Mech Phys Solids 1973;21:395.
[20] Parkins RN, Marsh GP, Evans JT. In: Okada H, Staehle R, editors. Predictive methods for assessing corrosion damage to BWR piping and PWR steam generators. Houston, TX: NACE; 1982. p. 249.
[21] Scully JC. Corros Sci 1980;20:997.
[22] Ford FP. In: Gangloff RP, Ives MB, editors. Environment-induced cracking of metals. Houston, TX: NACE; 1990. p. 139.
[23] Ford FP, Andresen PL. In: Bruemmer SM, Meletis EI, Jones RH, Gerberich WW, Ford FP, Staehle RW, editors. Parkins symposium on fundamental aspects of stress corrosion cracking. Warrendale, PA: TMS; 1992. p. 43.
[24] Hall MM. In: Shipilov SA, Jones RH, Olive J-M, Rebak RB, editors. Environment-induced cracking of materials, vol. 1. Oxford: Elsevier; 2008. p. 59.
[25] Hall MM. Corros Sci 2008;50:2902.
[26] Warner JS, Kim S, Gangloff RP. Int J Fatigue 2009;31:1952.
[27] Ritchie RO. In: Panontin TL, Sheppard SD, editors. Fatigue and fracture mechanics, ASTM STP 1332, vol. 29. West Conshohocken, PA: ASTM; 1999. p. 552.
[28] Ritchie RO. Int J Fract 1999;100:55.
[29] Stewart AT. In: Swann PR, Ford FP, Westwood ARC, editors. Mechanisms of environment sensitive cracking of materials. London: The Metals Society; 1977. p. 400.
[30] Shih T-H, Wei RP. Eng Fract Mech 1983;18:827.
[31] Gangloff RP. In: Gangloff RP, Ives MB, editors. Environment-induced cracking of metals. Houston, TX: NACE; 1990. p. 55.
[32] Davidson DL, Lankford J, Yokobori T, Sato K. Int J Fract 1976;12:579.
[33] Davidson DL, Lankford J. Int Mater Rev 1992;37:45.
[34] Weir TW, Simmons GW, Hart RG, Wei RP. Scripta Metall 1980;14:357.
[35] Marrero TR, Mason EA. J Phys Chem Ref Data 1972;1:1.
[36] Kestin J et al. J Phys Chem Ref Data 1984;13:229.
[37] Graat PCJ, Somers MAJ. Appl Surf Sci 1996;100/101:36.
[38] Avila K, Moxey D, de Lozar A, Avila M, Barkley D, Hof B. Science 2011;333:192.

Please cite this article in press as: Somerday BP et al. Elucidating the variables affecting accelerated fatigue crack growth of steels in hydrogen gas with low oxygen concentrations. Acta Mater (2013), http://dx.doi.org/10.1016/j.actamat.2013.07.001